Analytical Methods

ROYAL SOCIETY OF CHEMISTRY

TECHNICAL NOTE

View Article Online
View Journal | View Issue

Cite this: *Anal. Methods*, 2025, **17**, 8828

Characterizing nanoparticle size and composition using microfluidic Raman diffusion-ordered spectroscopy

Robert W. Schmidt, †[ab] Giulia Giubertoni,†*[b] Paul Kolpakov,[c] Noushine Shahidzadeh,[c] Freek Ariese *[a] and Sander Woutersen *[b]

Received 28th July 2025
Accepted 15th October 2025

DOI: 10.1039/d5ay01250c

rsc.li/methods

We show that microfluidic Raman Diffusion-Ordered SpectroscopY (Raman-DOSY) can be used to simultaneously characterize the size and the chemical composition of nanoparticles in solution. In these experiments, we inject a solution of nanoparticles into one half of a microfluidic channel, and solvent into the other. After the injection, the nanoparticles diffuse from the solution-filled part into the solvent-filled part of the channel, at a rate determined by their diffusion coefficient. By analyzing the time-dependent Raman spectrum in the initially solvent-filled part of the channel, we determine the size (from the diffusion coefficient) and characterize the chemical composition (from the corresponding Raman spectra) of the nanoparticles. Within about 1 hour we obtain both the size and chemical-structure information of polystyrene beads with diameters of 20, 50, and 100 nm. We further demonstrate that this method can distinguish nanoparticles of varying sizes in mixed samples. These results show that microfluidic Raman-DOSY is a promising method for combined size- and composition analysis of nanoparticles.

Introduction

Characterizing the chemical structure and determining the size of nanoparticles in solution is essential in many industrial and academic applications, including nanoparticle-based advanced materials, drugs, and biomedical diagnostics.[1–6] Among the available techniques to characterize the chemical structure of nanoparticles, Raman spectroscopy is particularly valued for its label-free detection capabilities. It can provide chemical identification,[7–9] and does not require any special preparation or labeling of the sample, making it highly versatile and non-destructive. Crystals and synthetic polymers often exhibit distinct and intense Raman signals, allowing for the precise identification and analysis of nanocrystals[10] and nanoplastics.[11–13] However, for nanoparticles that are smaller than the optical-diffraction limit, Raman spectroscopy provides no information about the particle size.

To add size sensitivity to Raman spectroscopy, we have recently developed Raman Diffusion-Ordered Spectroscopy (Raman-DOSY), an analytical method that simultaneously measures the Raman spectrum and the diffusion coefficient of molecules (or particles) in a fluid, using the Stokes–Einstein relation to determine their sizes. We applied this technique to cytochrome-c, micelles, and acetonitrile, demonstrating its capability to characterize both biological and synthetic systems across a broad range of sizes.[14] Inspired by NMR-DOSY,[15–29] Raman-DOSY differs in its practical implementation while retaining the core concept of diffusion-based size estimation. Previous studies have explored diffusion mechanisms in polymer blends using confocal Raman microscopy and surface-enhanced Raman spectroscopy (SERS), particularly in polystyrene/polystyrene bilayer systems.[30–33]

In Raman-DOSY, the sample solution and the pure solvent are injected in parallel into a Y-shaped flow cell (Fig. 1A). The flow is laminar, resulting in a well-defined interface between the solution- and solvent-filled halves of the channel. The injection is stopped at $t = 0$, and subsequently a time series of Raman spectra is measured at the far edge of the solvent-filled half of the channel (Raman-laser focus indicated by the green spot in Fig. 1A). At $t = 0$, the Raman spectrum shows only the peaks of the solvent (and of the flow-cell substrate), but as time progresses, the Raman peaks of the diffusing solute molecules or particles appear with a time dependence that is determined by their diffusion coefficient. When analyzing a mixture of molecules/particles with different sizes, the smaller particles quickly diffuse into the laser spot ($t = t_1$), whereas the larger particles have a longer lag phase ($t = t_2 > t_1$), see Fig. 1B. From a global analysis of the two-dimensional frequency- and time-

[a]*LaserLaB Amsterdam, Department of Physics and Astronomy, Vrije Universiteit Amsterdam, De Boelelaan 1081, 1081 HV Amsterdam, the Netherlands. E-mail: f.ariese@vu.nl*

[b]*Van 't Hoff Institute for Molecular Sciences, University of Amsterdam, Science Park 904, 1098XH Amsterdam, the Netherlands. E-mail: g.giubertoni@uva.nl; s.woutersen@uva.nl*

[c]*Van der Waals-Zeeman Institute (WZI), Institute of Physics, University of Amsterdam, Science Park 904, 1098XH Amsterdam, The Netherlands*

† These authors contributed equally to this work.

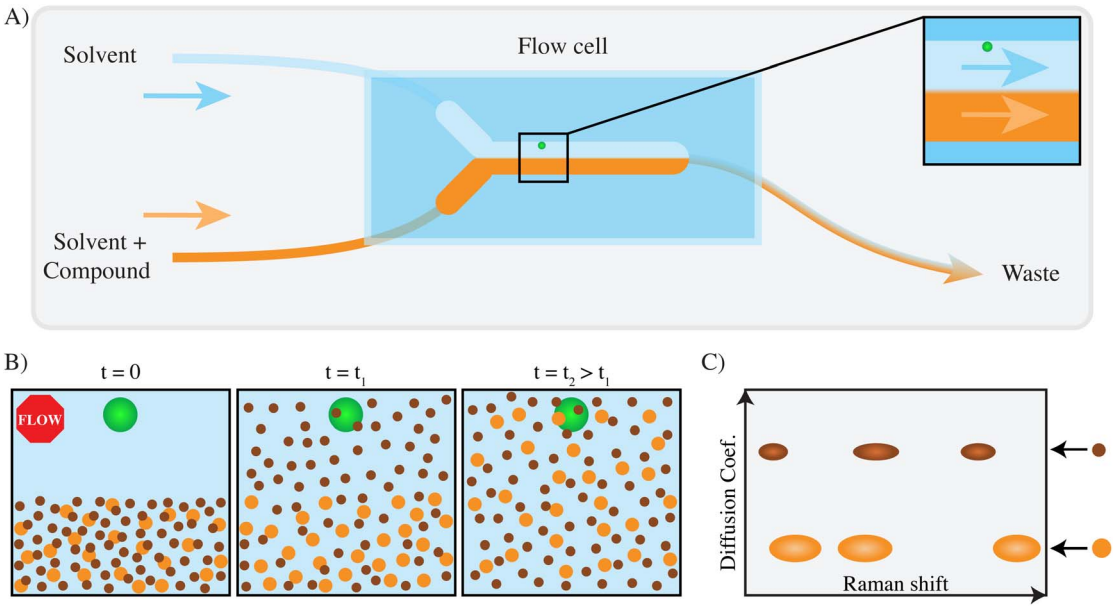

Fig. 1 (A) Schematic of a micro Raman DOSY experiment. The microfluidic flow cell has two inlets: one for the solvent and one for the sample solution. These are pumped into the cell to establish a stable laminar flow. The flow is stopped by stopping the pump, after which a time series of Raman spectra is measured at the outer edge of the initially solvent-filled part of the channel (indicated by the green laser spot). (B) After stopping the flow at $t = 0$, the solute molecules diffuse into the solvent-filled part of the channel and reach the detection location. Larger molecules diffuse at a slower rate than small ones. (C) Schematic Raman-DOSY plot derived from time-dependent data, displaying the Raman spectra of two compounds ordered by their diffusion coefficients.

dependent data set, we obtain a two-dimensional DOSY plot,[14] which has Raman frequency on the x axis and the diffusion coefficient (or equivalently, size) on the y-axis (Fig. 1C).

So far, we have applied Raman-DOSY only to small molecules and micelles, using a comparatively wide (4 mm) channel.[14] However, for larger particles diffusion over such a distance takes prohibitively long: a Raman-DOSY measurement would require several days for particles of 100 nm size in a channel of 4 mm width. However, the time required for an optical DOSY experiment scales with the square of the channel width (L^2), and therefore can be reduced by decreasing the channel width. Here, we go to the extreme limit of this idea by using a microfluidic approach to Raman-DOSY, with a 300 μm wide channel that enables us to determine the size and characterize the chemical structure of nanoparticles within a reasonable measurement time: approximately 2 hours for 100-nm particles, and less than 20 minutes for 20-nm particles in water.

Methods

Experiment

Sample preparation. All standards were obtained from Thermo Fisher and were part of the 3000 Series Nanosphere™ Size Standards series consisting of polystyrene spheres dispersed in water with added trace amounts of surfactant and sodium azide. The diameters of the spheres were calibrated to NIST standards by Thermo Fisher, resulting in a slight change in diameter compared to their nominal catalog values. The 20-nm polystyrene sphere standard had a measured size of 22 ± 2 nm diameter and a non-specified size distribution (catalog #3020 A). The 50-nm size standard consisted of spheres with a diameter of 51 ± 3 nm and a size distribution of 8.4 nm, std. dev. of 6.5% CV (catalog #3050 A). The 100-nm standard had a diameter of 101 ± 3 nm with a size distribution of 6.2 nm, std. dev. of 6.1% CV (catalog #3100 A). All standards initially contained 1% solids. To concentrate them, we placed an aliquot in a cuvette and incubated it in an oven at 50 °C until the concentration increased threefold. In all experiments, MilliQ water was used as the solvent.

Raman-DOSY setup. The custom-built setup to perform Raman-DOSY comprises of a microfluidic chip with an H-shaped channel chip (fluidic design 164, ChipShop) completely made from Topas (cyclic olefin copolymer) with a channel width of 300 μm and depth of 75 μm (Fig. 1A), a syringe pump (New Era Pump Systems, model 1000) and a customized connecting interface necessary to perform Optical-DOSY. In all experiments, the solvent and mixture were injected using two 100 μl Gastight 1/4-28 UNF glass syringes (Hamilton) at a flow rate of 2 μl min^{-1} (total flow in the cell 4 μl min^{-1}); the laminar flow is shown in Fig. S1. The Reynolds number calculated for the cell is Re ∼ 0.36, which puts the flow in the main chamber well within the highly laminar regime (Re < 1).[34]

Raman microscopy. Confocal Raman microscopy experiments were performed on a Renishaw inVia microscope system, equipped with a 63× Leica objective (HC PL FLUOTAR L, NA 0.70). The samples were excited with a 532-nm laser, and the back-scattered light was analyzed with a 1800 g mm^{-1} diffraction grating. The time series were continuously acquired with an exposure time of 1 second. Measurements of 100-nm

particles included a pause of either 0.25 or 1 s between measurements to allow the laser shutter to block the laser to avoid optical trapping of particles.

Data analysis

The Raman spectral pre-processing and data analysis were performed in MATLAB R2021b (The MathWorks Inc., Natick). Pre-processing included correcting spectral offsets by estimating a baseline (1-order polynomial and asymmetric truncated quadratic cost function),[35] and removing the Raman peaks associated with the water and flow-cell substrate by averaging the first three spectra of a time series to create a blank spectrum and subtracting that from the entire dataset.

Spectral processing and diffusion length determination. To accurately determine the diffusion coefficient, it is essential to precisely measure the length over which the particles diffuse to reach the detection point. To determine this diffusion length, we performed a line scan over the channel in 5 μm steps perpendicularly to the flow direction while the solvent and the mixture were pumped through the channel. The spectral dataset was pre-processed by truncating the spectra around the polystyrene peak at 1001 cm^{-1} (990 to 1013 cm^{-1}) and correcting baseline offsets as described above.[35] The peak area was derived and mapped relative to the cell coordinates, providing spatial details regarding the location of the cell and the interface between the sample channel and the water channel. Additionally, the Savitzky–Golay filter was employed to reduce the high-frequency noise in the plotted peak area *vs.* cell coordinates, caused by particles rapidly moving through the focal volume of the laser (see Fig. S7). The position of the interface was then determined by fitting the spatial Raman intensity profile during injection (Fig. S2) with an expression that is commonly used to determine the size of a laser spot: $1 - \mathrm{erf}(\sqrt{2}(x - x_0)/w)$, where x_0 is the position of the interface and w is the radius ($1/e^2$) of the estimated Gaussian laser spot. The diffusion distance was calculated from the interface location including the radius to the laser location.

Spectral processing of time-dependent datasets. Occasional trapping of particles in the optical volume of the laser causes distorted spectra in the time series. These spikes are removed using the Hampel filter, implemented in MATLAB's "filloutliers" function. Outliers are flagged if they lie beyond three times the local mean absolute deviation from the local median of a 300-length window, and then the flagged outliers are replaced by the median value of that window, see Fig. S7. This method also corrects for cosmic rays. Additionally, the data set was normalized to a range of 0 to 1 by dividing each value of the data set by the mean of the last 20 measurements.

The method for calculating the diffusion coefficient is described in detail elsewhere.[14,36] In short, the diffusion is described by the diffusion equation:

$$\frac{\partial c(y,t)}{\partial t} = D\frac{\partial^2 c(y,t)}{\partial y^2} \tag{1}$$

where D is the diffusion coefficient. At $t = 0$, the concentration in the channel can be described by a step function between the sample and solvent flows, where the liquid–liquid interface is at $y = 0$. With the initial concentration profile defined as $c(y, 0) = 1$ for the sample flow region ($-L/2 \le y < 0$) and $c(y, 0) = 0$ for the solvent flow region ($0 \le y \le L/2$) within the channel, where L represents the total width of the channel. In our experiments, we measure the Raman signal at the channel's far edge ($y = L/2$), where the time-dependent concentration is $c(L/2, t)$. By defining a dimensionless time variable $\tau = Dt/L^2$, we can write $c(L/2,t) = C(\tau)$, where $C(\tau)$ is a function solely determined by the dimensionless parameter τ.[36] Full summation expressions for C are given in ref. [36]. For practical applications, we can attain a relative precision of 10^{-8} using

$$C(\tau) = \begin{cases} 0 & \text{if } \tau = 0 \\ \frac{1}{2} - \frac{1}{2}\sum_{n=-3}^{3}(-1)^n \mathrm{erf}\left(\frac{n+1/2}{2\sqrt{\tau}}\right) & \text{if } 0 < \tau < 0.2 \\ \frac{1}{2} - \frac{2}{\pi}e^{-\pi^2\tau} & \text{if } \tau \ge 0.2, \end{cases} \tag{2}$$

where erf(x) is the error function.

The time- and frequency-dependent Raman spectra S were measured at the far edge ($y = L/2$) of the channel and were globally fitted to the following function to obtain the diffusion coefficients and associated spectra:

$$S(\nu, t) = \sum_{i=1}^{N} S_i(\nu) C\left(D_i t/L^2\right), \tag{3}$$

where N is the number of components in the sample (in our experiments $N = 1$, 2 or 3), Si(ν) denotes the Raman spectrum for the ith species, D_i the diffusion coefficient of species i, and $C(\tau)$ is given by eqn (2), depending solely on the reduced time $\tau = Dt/L^2$. In the global-fitting routine, we begin by fitting at a single Raman frequency (single-frequency fit) to obtain rough estimates for the diffusion coefficients that are then used as initial values for these parameters in the global fit. For the initial values of the spectral amplitudes we use the spectral intensities at the longest observed time. In the case of the triple mixture containing 100 nm particles, 20 nm particles, and contaminant, it is important to choose reasonable initial values for the fit parameters to guarantee convergence of the global fit to the overall chi-square minimum. We set the initial spectral amplitudes for the 100 nm and 20 nm components to the experimentally observed long-time experimental values, and for contaminant to 10% of the long-time values to account for its lower abundance (as determined from the measurement on the 100 nm sample).

To obtain a 2D DOSY spectrum $I(\nu, D)$ from the global-fit result, we multiply the spectral amplitude $S_i(\nu)$ by the appropriate probability distribution for D_i:[37]

$$I(\nu, D) = \sum_{i=1}^{N} S_i(\nu)\frac{e^{-(D-D_i)/2\sigma_i^2}}{\sqrt{2\pi\sigma_i}}, \tag{4}$$

where N represents the total number of components and σ_i denotes the uncertainties in the diffusion coefficients D_i, as obtained from averaging over multiple independent experiments. All measurements used for averaging are provided in the

supplementary material. The sphere diameters were calculated using the Stokes–Einstein equation at 21 °C, assuming the viscosity of water to be 1 mPa s.

Results

Microfluidic Raman DOSY on monodisperse nanoparticles

We use polystyrene beads to investigate the capability of microfluidic Raman DOSY for characterizing nanoplastic particle size and composition. Polystryene has a pronounced Raman peak at 1001 cm^{-1} (due to the trigonal phenyl-ring breathing mode) and a less intense peak at 1031 cm^{-1} (due to the CH_2-rocking mode).[38,39] Fig. 2A shows the time series of Raman spectra observed upon injecting a suspension of 51-nm polystyrene beads into the microfluidic DOSY cell (substrate and water Raman signals subtracted), with the spectral curves transitioning in color from blue (first spectrum) to red (last spectrum). Fig. 2B and C (top panels, blue curves) shows the spectrally integrated Raman intensity as a function of time (spectral integration range 993–1010 cm^{-1}). The time dependence mirrors the diffusion of the nanoparticles into the top part of the channel, which occurs much more slowly for the larger particles (note the different axis ranges). The red curves in the plots are least-squares fits of eqn (2) to the data. From a global least-squares fit of eqn (3) to the data we obtain Raman-DOSY spectra, shown in the bottom panels of Fig. 2. These spectra show the two characteristic Raman peaks of polystyrene (1001 and 1031 cm^{-1}), together with the diffusion coefficients (the standard deviations in the latter were obtained by performing three independent measurements; the separate measurements are shown in Fig. S3), from which we can estimate the particle size.

From the Raman-DOSY measurement, we obtain a diffusion coefficient of $1.86 \pm 0.1 \cdot 10^{-7}$ cm^2 s^{-1} for the 22-nm polystyrene beads, which is slightly lower than the expected diffusion coefficient of $1.96 \cdot 10^{-7}$ cm2, but within the uncertainty range. From the observed diffusion coefficient, we estimate the size to be 23.6 ± 1.1 nm (1σ), which is within the error margin of the certified size of 22 ± 2 nm. The 51-nm Raman-DOSY measurements yielded a diffusion coefficient of $7.58 \pm 0.06 \cdot 10^{-8}$ cm^2 s^{-1}, which is slightly lower than the expected diffusion coefficient of $8.45 \cdot 10^{-8}$ cm^2 s^{-1}. The size estimated from the Raman-DOSY measurement is 58 ± 3 nm (the individual time-dependent plots of the triplicate measurement used to determine the uncertainties in the diffusion constant and the size are shown in Fig. S4).

Microfluidic Raman DOSY on mixed nanoparticle solutions

We have also investigated the suitability of microfluidic Raman DOSY to characterize samples containing nanoparticles of more than one size. For this purpose, we prepared a mixture of 20 nm and 100 nm polystyrene beads. Interestingly, from our Raman-DOSY measurement on the pure standards we found that the 100 nm polystyrene standard contained an impurity with a much smaller size: the time-dependent Raman signal of the 100 nm polystyrene standard, shown in the top panel of Fig. 3A, is a sum of two sigmoidal curves, indicating the presence of two very different sizes in the sample. The smaller particles diffuse within about 15 s, after which the Raman signal curve rises further until it reaches a plateau level at around 5000 s. We could fit the time-dependent Raman signal of the 100 nm standard using a sum of two components (eqn (3) with $N = 2$; the data could not be described by a single-component fit, see

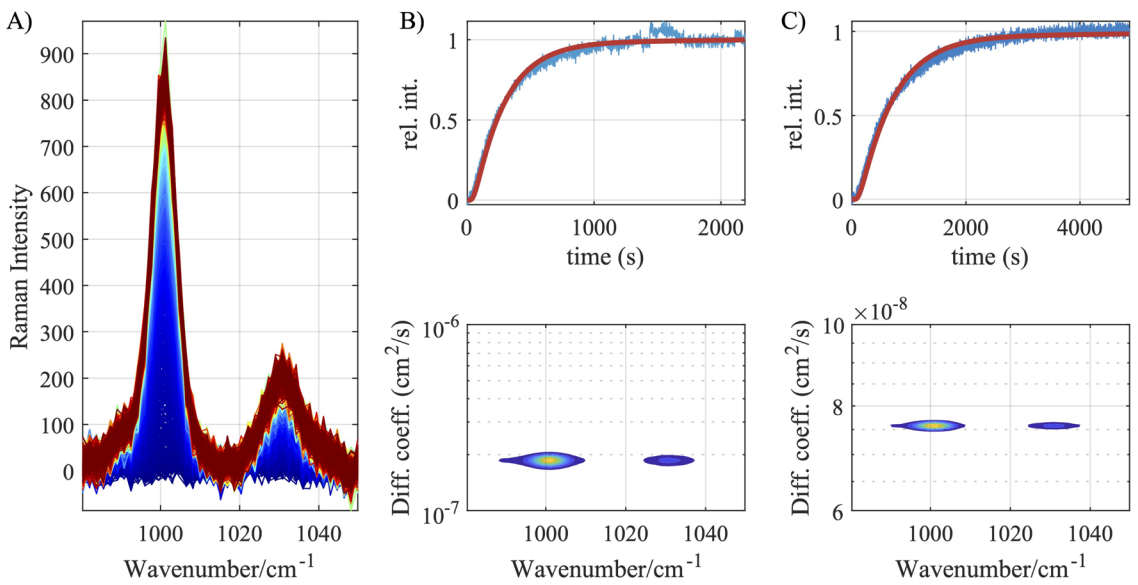

Fig. 2 Raman diffusion-ordered spectroscopY of polystyrene nanospheres of 22 nm and 51 nm. (A) Time series of Raman spectra for 51 nm polystyrene beads, color-coded from blue ($t = 0$) to red ($t = 4867$ s). The peak at 1001 cm^{-1} was integrated and used for the time-dependent plots shown in (B) and (C) top panels. Time-dependent plots (top panels) and Raman-DOSY plots (bottom panels) for (B) 22-nm and (C) 50-nm nanoplastic beads. The top panels display the growth of the integrated peak at 1001 cm^{-1} (blue) and a least-squares fit to obtain the diffusion coefficient (red). Bottom panels: Raman-DOSY spectra of polystyrene nanoparticles obtained from the global fit of the data obtained in the time-series measurements.

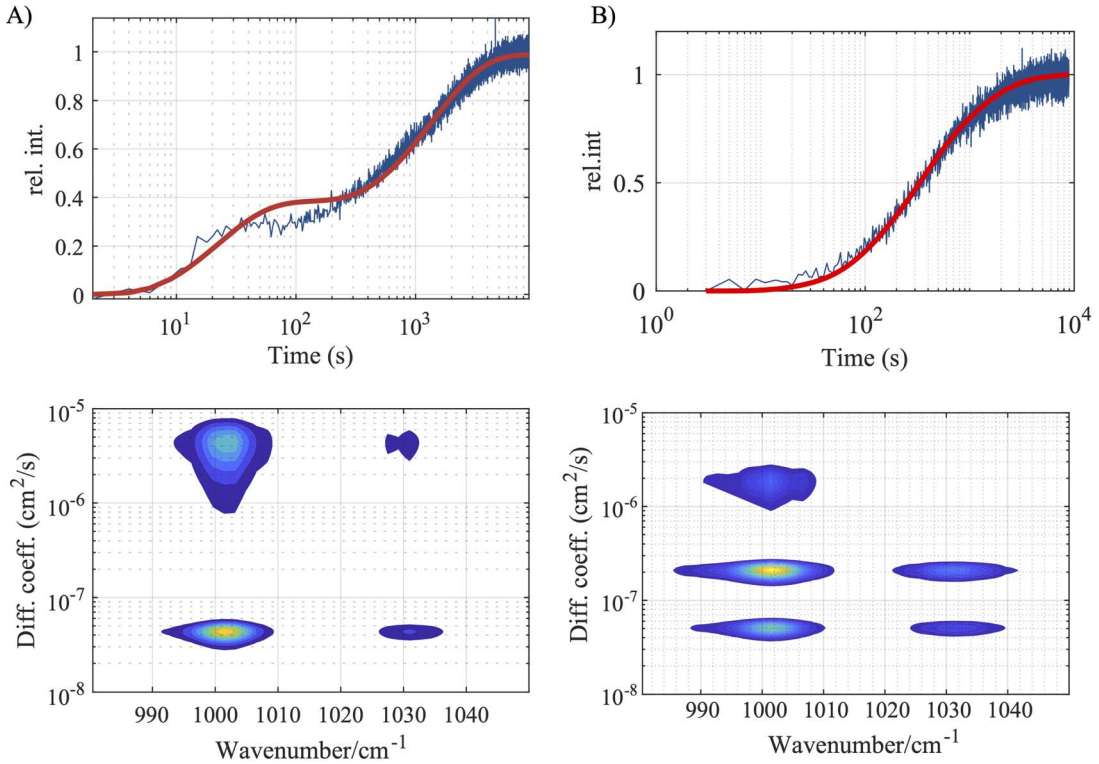

Fig. 3 Time-dependent and Raman-DOSY plots of polystyrene mixtures of (A) 100-nm spheres and ≈ 1-nm impurity, and (B) 20 nm and 100 nm spheres. Top panels: the blue curves show the time-dependent frequency-integrated intensity of the peak at 1001 cm^{-1}. The red curves are the result of a least-squares fit, using the diffusion coefficients and amplitudes as the fitting parameters. Bottom panels: Raman-DOSY spectra obtained from the global fit of the time series of Raman spectra, showing two or three distinct sizes with their corresponding Raman spectra. The DOSY plots were obtained from the mean diffusion coefficients and standard deviations resulting from five independent measurements for the 100 nm sample (A) and three independent measurements for the 20 nm and 100 nm mixture (B).

Fig. S10. From five independent measurements (see SI), we estimate a mean diffusion coefficient for the smaller compound of $4.35 \pm 1.93 \cdot 10^{-6}$ cm^2 s^{-1}, while for the larger it was $4.34 \pm 0.66 \cdot 10^{-8}$ cm^2 s^{-1}, which corresponds to a mean size of 1.0 ± 0.4 nm and 101 ± 15 nm, respectively; see Table S1 and Fig. S5. The corresponding DOSY plot (Fig. 3A, bottom) also shows the two compounds, which have an identical Raman spectrum but very different diffusion coefficients (y-coordinates). Since the initial diffusing impurity in the 100 nm standard was not specified in the polystyrene standard, we aimed to identify it. The Raman spectra of both compounds exhibited peaks at 622, 1001, 1030, 1159, and 1602 cm^{-1}, which matched the Raman spectra of polystyrene used in the nanosphere standard. Additionally, we applied Principal Component Analysis (PCA) to illustrate the variance during the diffusion of the compounds (see Fig. S8). To this purpose, we divided the entire spectral time series dataset into two subsets, one for each compound, and applied PCA to these datasets. The plots of the principal components for the impurity and the 100-nm beads dataset were nearly identical, except for the noise. The absence of missing or shifted peaks suggests that the impurity is a polystyrene oligomer, with a diameter of 1.0 ± 0.4 nm (corresponding to ~351 Da, using $\rho = 1.05$ g cm^{-3}). The 1 nm sized impurity was not observed in the 50 nm and 20 nm polystyrene standards (Fig. S9).

We then analyzed a (1 : 1 v/v) mixture of polystyrene beads with specified diameters of 22 nm and 101 nm. The time-dependent Raman signal is shown in Fig. 3B (triplicate measurement shown in Fig. S6). From a global least-squares fit of eqn (3) to the time- and frequency dependent data, in which we include the abovementioned contamination as the third component, we obtain diffusion coefficients $2.1 \pm 0.3 \cdot 10^{-7}$ cm^2 s^{-1} for the nominally 20-nm beads and $5.1 \pm 0.6 \cdot 10^{-8}$ cm^2 s^{-1} for the nominally 100 nm beads (these values are averages and standard deviations obtained from three independent measurements), from which we estimate diameters of 20.6 ± 2.6 nm and 84 ± 10 nm. These estimated diameters are somewhat smaller than the specified sizes of 22 and 101 nm, possibly due to cross-correlation between the two size parameters in the global least-squares fit: the overlapping diffusion curves of the two particles make it challenging for the fitting algorithm to accurately separate and fit the data for each compound. We are currently working on improved algorithms based on NMR-DOSY methods[40–43] to improve the accuracy of our data analysis.

Discussion

The above results show that microfluidic Raman DOSY can be used for characterizing the size (from the diffusion coefficients) and chemical structure (from the associated Raman spectra) of nanoparticles. Thus microfluidic Raman DOSY forms a simple

and affordable complement to the existing methods for nanoparticle analysis, the most important of which we will now discuss briefly.

NMR-DOSY efficiently measures the diffusion coefficient of particles and simultaneously provides their NMR spectrum,[25,37,44–46] but also has some drawbacks: for large particles, line broadening makes it difficult to record NMR-DOSY spectra, and moreover, NMR requires the use of deuterated solvents. Electron microscopy (SEM) is another commonly used method to determine particle sizes. The size resolution is about 1 nm, rendering it very suitable for nanoparticles but rather impractical to precisely determine the dimensions of small polymers or oligomeric contaminations. When combined with energy-dispersive X-ray spectroscopy, it can identify compounds based on their elemental composition. Although effective for analyzing nanoplastics, it is time-consuming, and it only provides a local size distribution.

Chromatography methods such as size exclusion chromatography (SEC) and field flow fractionation (FFF) are also often used to determine particle sizes.[47,48] Different types of detectors can be combined with SEC, but in general they provide rather limited information on the chemical composition of the particles.

FFF combined with a multi-angle light scattering detector can measure colloids down to 50 nm but does not provide chemical identification.[49,50] Using SEC and FFF combined with mass spectrometry has shown success in characterizing proteins and biopharmaceuticals,[51] although accessibility may vary depending on laboratory infrastructure. Other size-sensitive methods are dynamic light scattering (DLS) and nanoparticle tracking analysis (NTA).[52–54] These purely size-sensitive methods can determine accurate size distributions across the sample but need to be combined with another technique to identify the chemical structure of particles.

Raman-DOSY probes the size and chemical structure simultaneously, and thus offers a reliable and non-invasive method to investigate and characterize nanoparticles. Unlike chromatography or NMR-DOSY, Raman-DOSY does not require calibration with standards of well-defined sizes, or the use of deuterated solvents. However, the limited sensitivity of Raman spectroscopy to detect molecules at low concentrations restricts the current application of Raman-DOSY. This low sensitivity is primarily due to the inherently weak Raman scattering, which is further reduced because the compounds of interest are diluted by a factor of two by the solvent channel in the cell during the measurement. An effective solution to this problem is to enhance the signal using resonance Raman spectroscopy.[55,56] This technique involves tuning the excitation wavelength to match an electronic transition of the molecule, significantly amplifying the Raman signal. Additionally, targeting specific vibrational modes, such as the CH stretches of the polymer backbone, can further improve the sensitivity. For molecules with inherently weak Raman cross section, techniques such as Stimulated Raman Scattering (SRS) spectroscopy can be employed to enhance sensitivity.[57] In cases where particles exhibit no detectable Raman signal, such as exosomes or metal oxide nanospheres, an alternative strategy might be to monitor the solvent. By measuring the reduction in the Raman signal of the solvent, one can in principle infer the presence of non-Raman-active particles, as they displace the solvent within the detection volume. However, in such cases other (UV/vis, IR) optical DOSY methods[36,58] might be more efficient.

Samples containing a large number of components, or a continuous size distribution, will be less easy to analyze than the test samples investigated here, but we believe that many data analysis methods that have been developed for NMR-DOSY measurements of such complicated samples[15,40,59–61] can also be used (after minor modifications) to analyze optical-DOSY measurements.

The applicability of microfluidic Raman-DOSY for nanoparticle analysis is currently limited somewhat by the window material (olefin polymer) used in our microfluidic DOSY cell and the analysis algorithm. Raman peaks of the particles may overlap with signals from the microfluidic window, making it difficult to distinguish between the sample and the cell material. Cell designs with glass, quartz or CaF_2 top or bottom windows will solve these issues. To improve the data analysis, we want to apply the advanced data-analysis methods that have been developed previously for NMR-DOSY, and that make it possible to characterize the size distribution of polydisperse samples in a robust manner.[40–43]

Conclusions and outlook

We have investigated solutions containing nanoplastic particles of different sizes using microfluidic Raman DOSY. By using a small channel width, we can investigate nanoparticles in a competitive timeframe, as demonstrated by the Raman-DOSY spectra of polystyrene beads with diameters of 20, 50, and 100 nm. At the same time, we can detect smaller impurities in the polystyrene standard, demonstrating that the method can be used to analyze samples with a wide particle size distribution. We found that this method can successfully characterize the size and the chemical structure of the tested nano-plastic samples, with an accuracy of ~10%. We believe that Raman-DOSY offers a noninvasive and label-free method to characterize simultaneously the chemical structure and the size of nanoparticles/aggregates, which constitutes an easy-to-use and affordable addition to the existing methods for nanoparticle size and structure characterization.

Conflicts of interest

G. Giubertoni and S. Woutersen are co-founders and shareholders of InspectT, a spin-off commercializing optical-DOSY technology. The remaining authors declare no competing interests.

Data availability

The data for this article are available at Zenodo at **https://doi.org/10.5281/zenodo.15798911**.

Supplementary information is available. See DOI: **https://doi.org/10.1039/d5ay01250c**.

Acknowledgements

This research received funding from The Netherlands Organization for Scientific Research (NWO) in the framework of the ENW PPP Fund for the top sectors (Grant 741.018.202 "Soft Advanced Materials") and from the Ministry of Economic Affairs in the framework of the "PPS-Toeslagregeling". GG is supported by NWO under project number VI.Veni.212.240.

Notes and references

1 V. Mailänder and K. Landfester, *Biomacromolecules*, 2009, **10**, 2379–2400.
2 E. Busseron, Y. Ruff, E. Moulin and N. Giuseppone, *Nanoscale*, 2013, **5**, 7098–7140.
3 P. D. Howes, R. Chandrawati and M. M. Stevens, *Science*, 2014, **346**, 1247390.
4 M. Kopp, S. Kollenda and M. Epple, *Acc. Chem. Res.*, 2017, **50**, 1383–1390.
5 S. Mourdikoudis, R. M. Pallares and N. T. K. Thanh, *Nanoscale*, 2018, **10**, 12871–12934.
6 M. Epple, V. M. Rotello and K. Dawson, *Acc. Chem. Res.*, 2023, **56**, 3369–3378.
7 E. Smith and G. Dent, *Modern Raman Spectroscopy*, Wiley, 2019.
8 L. Ettema, B. Lochocki, J. J. M. Hoozemans, J. F. de Boer and F. Ariese, *J. Opt.*, 2022, **24**, 054005.
9 P. Larkin, *Infrared and Raman Spectroscopy*, Elsevier, 2011, vol. 44, p. 085201.
10 M. Testa-Anta, M. A. Ramos-Docampo, M. Comesana-Hermo, B. Rivas-Murias and V. Salgueirino, *Nanoscale Adv.*, 2019, **1**, 2086–2103.
11 L. Zada, H. A. Leslie, A. D. Vethaak, G. H. Tinnevelt, J. J. Jansen, J. F. de Boer and F. Ariese, *J. Raman Spectrosc.*, 2018, **49**, 1136–1144.
12 J. R. Ferraro, K. Nakamoto and C. W. Brown, *Introductory Raman Spectroscopy*, Elsevier, 2nd edn, 2003.
13 J. Toporski, T. Dieing and O. Hollricher, *Confocal Raman Microscopy*, Springer International Publishing, Cham, 2nd edn, 2018, vol. 66.
14 R. W. Schmidt, G. Giubertoni, F. Caporaletti, P. Kolpakov, N. Shahidzadeh, F. Ariese and S. Woutersen, *J. Phys. Chem. A*, 2023, **127**, 7638–7645.
15 K. F. Morris and C. S. Johnson Jr, *J. Am. Chem. Soc.*, 1992, **114**, 3139–3141.
16 C. S. Johnson Jr, *Prog. Nucl. Magn. Reson. Spectrosc.*, 1999, **34**, 203–256.
17 L. Avram and Y. Cohen, *Angew. Chem., Int. Ed.*, 2005, **44**, 520–554.
18 D. Li, I. Keresztes, R. Hopson and P. Williard, *Acc. Chem. Res.*, 2008, **42**, 270–280.
19 G. A. Morris, in *Encyclopedia of Magnetic Resonance*, ed. R. K. Harris and R. E. Wasylishen, Wiley, Chichester, UK, 2009.
20 K. Salorinne, T. Lahtinen, J. Koivisto, E. Kalenius, M. Nissinen, M. Pettersson and H. Häkkinen, *Anal. Chem.*, 2013, **85**, 3489–3492.
21 L. Avram and Y. Cohen, *Chem. Soc. Rev.*, 2014, **44**, 586–602.
22 M. Foroozandeh, L. C. nar, L. G. Martins, D. Sinnaeve, G. D. Poggetto, C. F. Tormena, R. W. Adams, G. A. Morris and M. Nilsson, *Angew. Chem., Int. Ed.*, 2016, **55**, 15579–15582.
23 R. Evans and I. J. Day, *RSC Adv.*, 2016, **6**, 47010–47022.
24 G. Pagès, V. Gilard, R. Martino and M. Malet-Martino, *Analyst*, 2017, **142**, 3771–3796.
25 P. Groves, *Polym. Chem.*, 2017, **8**, 6700–6708.
26 G. D. Poggetto, L. Castañar, M. Foroozandeh, P. Kiraly, R. W. Adams, G. A. Morris and M. Nilsson, *Anal. Chem.*, 2018, **90**, 13695–13701.
27 M. Urbańczyk, Y. Kharbanda, O. Mankinen and V.-V. Telkki, *Anal. Chem.*, 2020, **92**, 9948–9955.
28 K. Kristinaityte, A. Mames, M. Pietrzak, F. F. Westermair, W. Silva, R. M. Gschwind, T. Ratajczyk and M. Urbańczyk, *J. Am. Chem. Soc.*, 2022, **144**, 13938–13945.
29 E. Ruzicka, P. Pellechia and B. C. Benicewicz, *Anal. Chem.*, 2023, **95**, 7849–7854.
30 A. C. D. Luca, G. Rusciano, G. Pesce, S. Caserta, S. Guido and A. Sasso, *Macromolecules*, 2008, **41**, 5512–5514.
31 C. D. Mana, G. A. Torchia and J. P. Tomba, *Soft Matter*, 2018, **14**, 3315–3323.
32 R. Demoor, V. Guarepi, A. Cisilino, V. Alvarez and J. P. Tomba, *J. Raman Spectrosc.*, 2021, **52**, 1022–1031.
33 A. P. Cisilino, C. D. D. Monno and J. P. Tomba, *Soft Matter*, 2024, **20**, 7535–7545.
34 F. M. White, *Fluid Mechanics*, McGraw-Hill, 7th edn, 2009.
35 V. Mazet, C. Carteret, D. Brie, J. Idier and B. Humbert, *Chemom. Intell. Lab. Syst.*, 2005, **76**, 121–133.
36 G. Giubertoni, G. Rombouts, F. Caporaletti, A. Deblais, R. van Diest, J. N. H. Reek, D. Bonn and S. Woutersen, *Angew. Chem., Int. Ed.*, 2023, **62**, e202213424.
37 K. F. Morris and C. S. Johnson, *J. Am. Chem. Soc.*, 1992, **114**, 3139–3141.
38 A. Palm, *J. Phys. Chem.*, 1951, **55**, 1320–1324.
39 C. H. Choi and M. Kertesz, *J. Phys. Chem. A*, 1997, **101**, 3823–3831.
40 M. A. Delsuc and T. E. Malliavin, *Anal. Chem.*, 1998, **70**, 2146–2148.
41 T. Buffeteau, L. Ducasse, L. Poniman, N. Delsuc and I. Huc, *Chem. Commun.*, 2007, 2714–2716.
42 M. Urbańczyk, D. Bernin, W. Koz&macute;iński and K. Kazimierczuk, *J. Phys. Chem. Lett.*, 2013, **85**, 1828–1833.
43 A. Cherni, E. Chouzenoux and M.-A. Delsuc, *Analyst*, 2017, **142**, 772–779.
44 X.-X. Zhang, S. L. Brantley, S. A. Corcelli and A. Tokmakoff, *Nat. Commun. Biol.*, 2020, **3**, 525.
45 M. S. Ullah, V. V. Zhivonitko, A. Samoylenko, A. Zhyvolozhnyi, S. Viitala, S. Kankaanpää, S. Komulainen, L. Schröder, S. J. Vainio and V.-V. Telkki, *Chem. Sci.*, 2021, **12**, 8311–8319.
46 N. Wolff, C. Beuck, T. Schaller and M. Epple, *Nanoscale Adv.*, 2024, **6**, 3285–3298.
47 H. G. Barth, C. Jackson and B. E. Boyes, *Anal. Chem.*, 1994, **66**, 595–620.
48 A. M. Striegel, *Chromatographia*, 2022, **85**, 307–313.

49 M. Baalousha, F. V. Kammer, M. Motelica-Heino, H. S. Hilal and P. Le Coustumer, *J. Chromatogr. A*, 2006, **1104**, 272–281.
50 J. Gigault, H. El Hadri, S. Reynaud, E. Deniau and B. Grassl, *Anal. Bioanal. Chem.*, 2017, **409**, 6761–6769.
51 C. Contado, *Anal. Bioanal. Chem.*, 2017, **409**, 2501–2518.
52 M. Kaszuba, D. McKnight, M. T. Connah, F. K. McNeil-Watson and U. Nobbmann, *J. Nanopart. Res.*, 2008, **10**, 823–829.
53 J. Stetefeld, S. A. McKenna and T. R. Patel, *Biophys. Rev.*, 2016, **8**, 409–427.
54 H. Jans, X. Liu, L. Austin, G. Maes and Q. Huo, *Anal. Chem.*, 2009, **81**, 9425–9432.
55 S. Chadha, E. Ghiamati, R. Manoharan and W. H. Nelson, *Appl. Spectrosc.*, 1992, **46**, 1176–1181.
56 A. H. Kuptsov and G. N. Zhizhin, *Handbook of Fourier Transform Raman and Infrared Spectra of Polymers*, Elsevier, 1998, vol. 45.
57 L. van Haasterecht, L. Zada, R. W. Schmidt, E. de Bakker, E. Barbé, H. A. Leslie, A. D. Vethaak, S. Gibbs, J. F. de Boer, F. B. Niessen, P. P. M. van Zuijlen, M. L. Groot and F. Ariese, *J. Biophot.*, 2020, **13**, 1–10.
58 G. Giubertoni, M. G. Rachid, C. Moll, M. Hilbers, S. Samanipour and S. Woutersen, *Anal. Chem.*, 2024, **96**, 15168–15176.
59 S. W. Provencher, *Comput. Phys. Commun.*, 1982, **27**, 213–227.
60 M. Nilsson and G. A. Morris, *Anal. Chem.*, 2008, **80**, 3777–3782.
61 A. A. Colbourne, S. Meier, G. A. Morris and M. Nilsson, *Chem. Commun.*, 2013, **49**, 10510–10512.